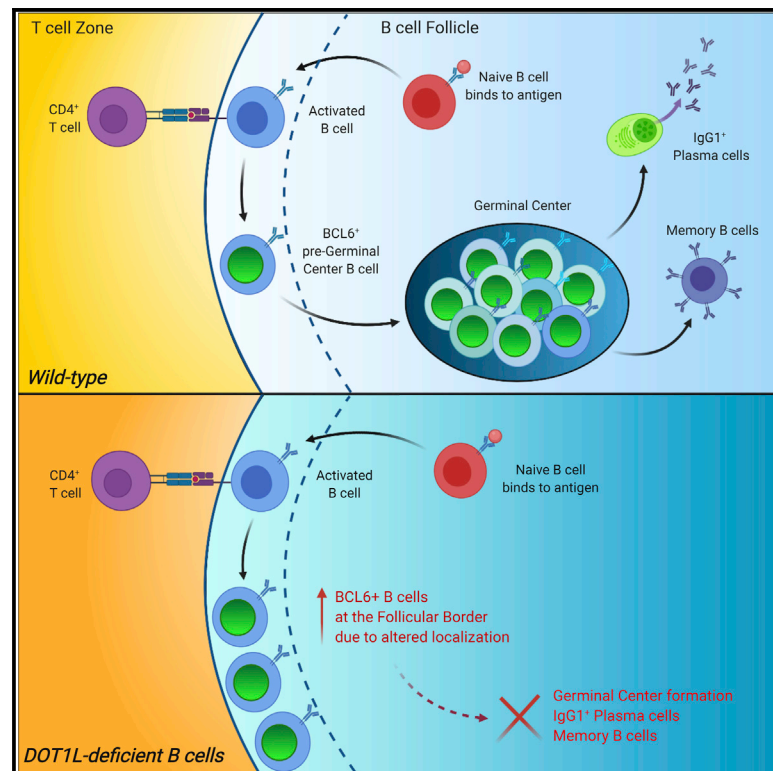# The Histone Methyltransferase DOT1L Is Essential for Humoral Immune Responses

Graphical Abstract

Authors

Liam Kealy, Andrea Di Pietro, Lauren Hailes, ..., Joanna R. Groom, Colby Zaph, Kim L. Good-Jacobson

Correspondence

kim.jacobson@monash.edu

In Brief

B cell differentiation is critical for antibody-mediated clearance of pathogens. Kealy et al. show a key role for the histone modifier DOT1L in B cell responses. DOT1L is essential for appropriate localization of B cells to form germinal centers, the critical sites for producing high-affinity antibody and B cell memory.

Highlights

- B cell fate in lymphoid organs is regulated by the histone modifier DOT1L

- DOT1L is required for B cell development in the bone marrow

- DOT1L is essential for germinal center formation during an immune response

- Localization of activated BCL6+ B cells is dysregulated in the absence of DOT1L

CellPress

Report

The Histone Methyltransferase DOT1L Is Essential for Humoral Immune Responses

Liam Kealy,[1,2] Andrea Di Pietro,[1,2] Lauren Hailes,[1,2] Sebastian Scheer,[1,2] Lennard Dalit,[3,4] Joanna R. Groom,[3,4] Colby Zaph,[1,2] and Kim L. Good-Jacobson[1,2,5,*]

[1]Department of Biochemistry and Molecular Biology, Monash University, Clayton, VIC 3800, Australia
[2]Infection and Immunity Program, Biomedicine Discovery Institute, Monash University, Clayton, VIC 3800, Australia
[3]Division of Immunology, Walter and Eliza Hall Institute of Medical Research, Parkville, VIC 3052, Australia
[4]Department of Medical Biology, University of Melbourne, Parkville, VIC 3010, Australia
[5]Lead Contact
*Correspondence: kim.jacobson@monash.edu
https://doi.org/10.1016/j.celrep.2020.108504

SUMMARY

Histone modifiers are essential for the ability of immune cells to reprogram their gene expression during differentiation. The recruitment of the histone methyltransferase DOT1L (disruptor of telomeric silencing 1-like) induces oncogenic gene expression in a subset of B cell leukemias. Despite its importance, its role in the humoral immune system is unclear. Here, we demonstrate that DOT1L is a critical regulator of B cell biology. B cell development is defective in Dot1l[f/f]Mb1[Cre/+] mice, culminating in a reduction of peripheral mature B cells. Upon immunization or influenza infection of Dot1l[f/f]Cd23[Cre/+] mice, class-switched antibody-secreting cells are significantly attenuated and germinal centers fail to form. Consequently, DOT1L is essential for B cell memory formation. Transcriptome, pathway, and histological analyses identified a role for DOT1L in reprogramming gene expression for appropriate localization of B cells during the initial stage of the response. Together, these results demonstrate an essential role for DOT1L in generating an effective humoral immune response.

INTRODUCTION

A successful antibody-mediated immune response leads to pathogen clearance and the formation of immune memory. These processes underpin the vast majority of vaccines (Good-Jacobson, 2018). The foundation for this success originates from the activation of a small number of antigen-specific naive B cells. After activation, B cell differentiation is instructed by specific molecular programs that regulate fate and function during an immune response. These programs are modulated by epigenetic regulators (e.g., histone modifiers, small interfering RNAs [siRNAs], and DNA methylases) and transcription factors working in concert to determine whether genes are activated or repressed without changes to the DNA sequence (Zhang and Good-Jacobson, 2019). Histone modifiers regulate chromatin accessibility, thereby regulating the accessibility of transcriptional machinery to their targets (Strahl and Allis, 2000). Importantly, the same histone modifiers emerging as important regulators of B cell differentiation can also become dysregulated in malignancies (Alberghini et al., 2015; Béguelin et al., 2013; Inaba et al., 2013). Thus, histone modifiers are therapeutically attractive to target with small molecule inhibitors (Arrowsmith et al., 2012). It is therefore important to understand the roles of histone modifiers in regulating B cell differentiation.

DOT1L (disruptor of telomeric silencing 1-like) is the sole known enzyme that methylates lysine 79 of histone H3

(H3K79) and is most well-known for its role in oncogenesis. Approximately 40% of pediatric leukemias have been linked to H3K79 methylation-mediated oncogenic gene expression (Worden et al., 2019). B cell acute lymphoblastic leukemia (B-ALL) is an aggressive malignancy that affects children and adults, with long-term survival rates of <40% (Geng et al., 2012). A prominent subtype is MLL (mixed lineage leukemia)-rearranged B-ALL (MLLr B-ALL). The defining feature of MLLr-ALLs is rearrangement of the epigenetic regulator MLL, which results in the binding of MLL with any 1 of over 50 fusion partners. Although this promiscuous partnering makes it difficult to find genuine therapeutic targets, another prominent feature of this leukemia is the recruitment of a second epigenetic regulator, DOT1L (Krivtsov et al., 2008; Okada et al., 2005). Malignant gene expression is driven by DOT1L activity: inactivation of DOT1L downregulates genes targeted by MLL-fusion protein complexes (Bernt et al., 2011). Thus, DOT1L inhibition has become a major focus of translational research and is now in phase I/II clinical trials. Despite the clear importance of this molecule, there is scant information on the role of DOT1L in lymphocyte development in primary lymphoid organs or differentiation during an immune response in the periphery.

Epigenetic regulation of B cell differentiation is a nascent field, with understanding mostly limited to the roles of the methyltransferase EZH2 (Béguelin et al., 2013; Caganova

et al., 2013), MLL2 (Zhang et al., 2015), demethylase LSD1 (Good-Jacobson, 2019; Haines et al., 2018; Hatzi et al., 2019), and acetyltransferase MOZ (Good-Jacobson et al., 2014) in germinal center (GC) biology. DOT1L was recently found to be expressed by human tonsillar and lymph node GC B cells (Szablewski et al., 2018). Differential H3K79 methylation on the *IgH* locus in plasma cells, compared to lipopolysaccharide (LPS)-activated B cells, has been hypothesized to mediate the transition from membrane-bound to secretory forms of immunoglobulin (Milcarek et al., 2011). Thus, given its prominent role in *MLL*r B-ALL, its expression by GC B cells, and its potential role in antibody production, we set out to investigate the function of DOT1L in B cell differentiation and function.

By generating mouse strains deficient in DOT1L in either developing or mature B cells, we describe functional roles for DOT1L in B cell differentiation in both primary and secondary lymphoid organs. Our experiments delineate DOT1L as a vital checkpoint molecule during an immune response, as evidenced by the abrogation of humoral responses *in vivo*. In particular, our study links histone modification to the regulation of the migration-related gene network and, ultimately, B cell positioning in the follicle. Together, these results reveal the absolute requirement for DOT1L for B cells to mount an effective immune response *in vivo*.

RESULTS AND DISCUSSION

DOT1L Is Required for B Cell Development

We first sought to determine whether DOT1L was required in B cell biology through the generation of $Dot1l^{f/f}Mb1^{Cre/+}$ mice in which exon 2 of *Dot1l* was excised upon *Igα* expression (Figure S1A). Spleens from $Dot1l^{f/f}Mb1^{Cre/+}$ mice were notably smaller than those from $Mb1^{Cre/+}$ control mice (Figures S1B and S1C), and the B cell population was significantly reduced in $Dot1l^{f/f}Mb1^{Cre/+}$ mice compared to both $Dot1l^{f/+}Mb1^{Cre/+}$ and $Mb1^{Cre/+}$ controls (Figure S1D). Histological analyses revealed DOT1L-deficient mice were able to form follicular structures; however, a thinner marginal zone structure was clearly evident (Figure S1E). Correspondingly, both splenic marginal zone and follicular B cells were significantly decreased (Figures S1F–S1I), as were antibodies of all isotypes (Figures S1J–S1O).

Thus, it appeared that DOT1L was required for effective production of B cells to populate secondary lymphoid organs, such as the spleen. To investigate, we compared B cell subsets in the bone marrow (BM) of $Dot1l^{f/f}Mb1^{Cre/+}$ and $Dot1l^{f/+}Mb1^{Cre/+}$ to $Mb1^{Cre/+}$ controls. DOT1L deficiency resulted in a clear decrease of B cells (Figure 1A). In keeping with the deletion of *Dot1l* at the pro-B cell stage in this conditional deletion, there was no significant change in pro-B cells (Figure 1B). There was, however, a ~3-fold significant decrease in both the frequency (data not shown) and number (Figure 1B) in all subsequent developing B cell subsets. Furthermore, in most instances, mice heterozygous for the floxed allele suggested a gene dosage effect of DOT1L during the development of B cells. These data demonstrate an essential requirement for DOT1L during B cell development in the BM and thus the establishment of peripheral B cell populations.

DOT1L Is Essential for Formation of GCs

DOT1L was recently found to be expressed in a subset of human GC B cells, suggesting a role for DOT1L in the GC (Szablewski et al., 2018). The significantly reduced number of peripheral B cells in $Dot1l^{f/f}Mb1^{Cre/+}$ mice made the precise role of DOT1L in antigen-driven responses difficult to disentangle from the developmental defects in these mice. Therefore, we generated mice in which *Dot1l* is deleted specifically in mature B cells by crossing $Dot1l^{f/f}$ and $Cd23^{cre}$ mice. Thus, any phenotype in $Dot1l^{f/f}Cd23^{cre/+}$ mice should specifically be a consequence of the role of DOT1L in peripheral B cell differentiation and not due to the role of DOT1L observed during development in the BM (Figure S2A). $Cd23^{cre/+}$ and $Dot1l^{f/f}Cd23^{cre/+}$ mice were immunized with hapten (4-hydroxy-3-nitrophenyl)-acetyl conjugated to keyhole limpet hemocyanin (NP-KLH) precipitated on the adjuvant alum, and B cell responses were assessed. At day 7 (d7), control mice generated a discernible NP⁺CD95ʰⁱ GC B cell population (Figure 1C). In contrast, conditional deletion of DOT1L in B cells prohibited the formation of GC (Figure 1C). This was not due to delayed kinetics. Strikingly, GC B cell frequency (Figure 1D) and number (Figure 1E) were completely absent in $Dot1l^{f/f}Cd23^{cre/+}$ mice assessed during early (d7) and late (d28) phases of the response. Although the splenic morphology of B cell follicles appeared normal in $Dot1l^{f/f}Cd23^{cre/+}$ mice compared to $Cd23^{cre/+}$ controls (Figures 1F and 1G), histological analyses showed a complete lack of PNA⁺ GC (Figure 1F) and IgG1⁺ cells (Figure 1G). Therefore, DOT1L was essential for the formation of GC and IgG1⁺ B cells during an immune response to NP-KLH.

DOT1L Is Essential for the Establishment of Humoral Immunity

The formation of immune memory, consisting of memory B cells and long-lived plasma cells, is a critical outcome for an effective B cell response. In several gene-deficient models, the abrogation of GC responses is associated with an increase in early memory B cells (Good-Jacobson and Shlomchik, 2010). We therefore determined whether the absence of DOT1L affected the formation of immune memory subsets. Memory B cells, as defined by NP⁺IgG1⁺CD38⁺, were completely absent in DOT1L-deficient mice (Figure 1H). At both d7 and d28 post-immunization, memory B cell frequency (Figure 1I) and number (Figure 1J) were absent in $Dot1l^{f/f}Cd23^{cre/+}$ mice. Correspondingly, plasma cells in the BM (Figure 1K) were significantly decreased, with high-affinity antibody-secreting cells (ASCs) completely absent. As such, the circulating NP-binding IgG1 antibody was significantly decreased (Figure 1L). In addition to isotype-switched memory B cells, immunoglobulin M (IgM⁺) B cells constitute an important component of the memory B cell population (Dogan et al., 2009; Krishnamurty et al., 2016; Mesin et al., 2020; Pape et al., 2011). In the absence of the histone modifier MOZ (Good-Jacobson et al., 2014), a reduction in GC B cells was combined with an increase in IgM⁺ memory B cells. Therefore, we tested whether DOT1L deficiency similarly induced an increase in IgM⁺ memory. However, at d28 post-immunization, NP⁺IgM⁺CD38⁺ memory B cells were significantly decreased in $Dot1l^{f/f}Cd23^{cre/+}$ mice compared to $Cd23^{cre/+}$ mice (Figure S2B). Therefore, DOT1L
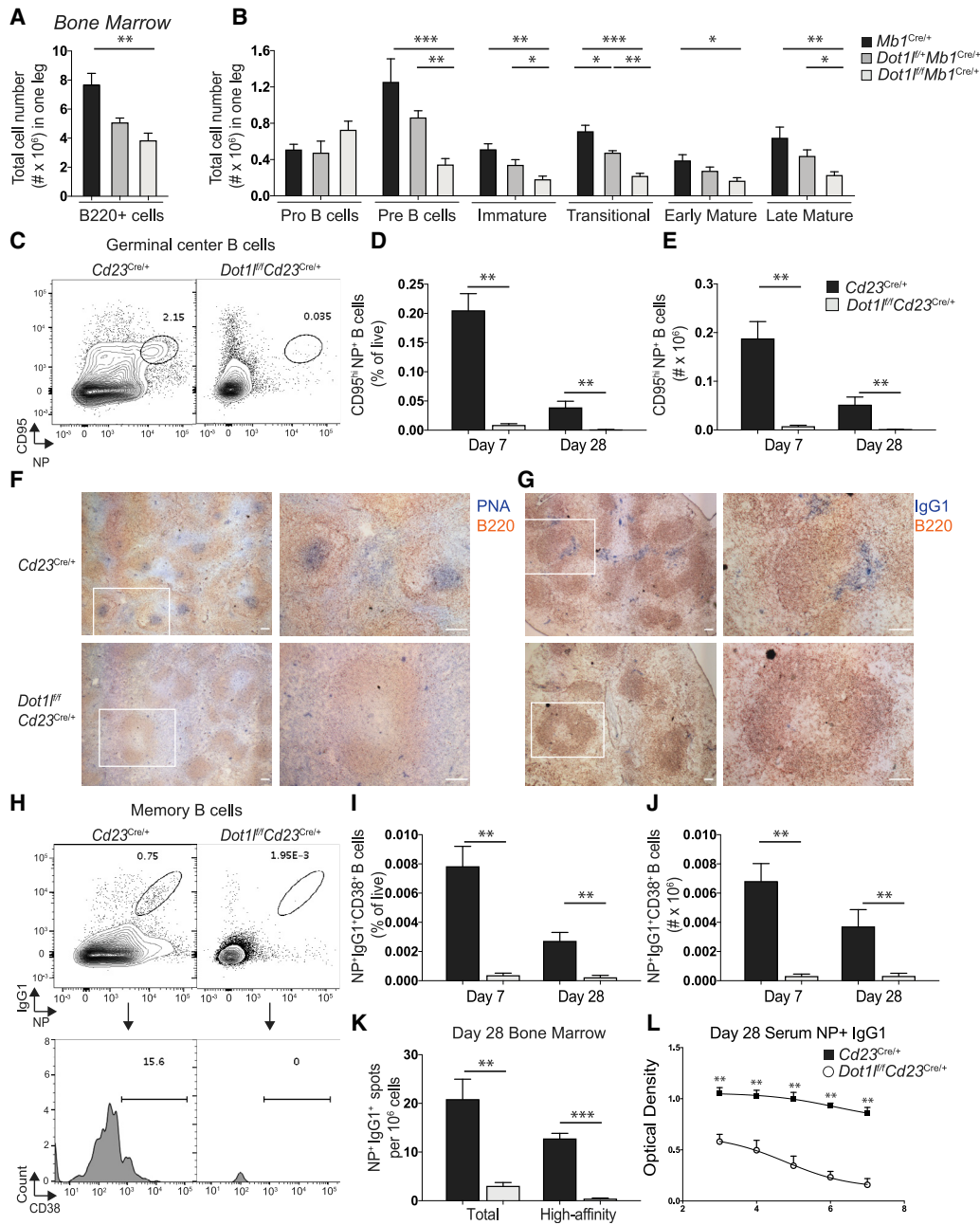
Figure 1. Dot1l Deletion Results in Ablation of GCs and Inability to Form Humoral Memory

(A and B) Flow cytometric analyses of BM B cell populations of naive, adult $Mb1^{Cre/+}$, $Dot1l^{fl/+} Mb1^{Cre/+}$, and $Dot1l^{fl/fl}Mb1^{Cre/+}$ mice. B220$^+$ populations (A) and pro-B cell (B220^{lo}CD24$^+$BP1$^-$CD43$^+$IgM$^-$), pre-B cell (B220^{lo}CD24$^+$BP1$^+$CD43$^-$IgM$^-$IgD$^-$), immature (B220$^+$CD24$^+$CD43$^-$IgM^{lo}IgD$^-$), transitional (B220$^+$CD24$^+$CD43$^-$IgM^{hi}IgD$^-$), early mature (B220$^+$CD24$^+$CD43$^-$IgM^{hi}IgD$^+$), and late mature (B220$^+$CD24$^+$CD43$^-$IgM^{lo}IgD$^+$) populations (B). $Mb1^{Cre/+}$ (n = 8), $Dot1l^{fl/+}Mb1^{Cre/+}$ (n = 5), $Dot1l^{fl/fl}Mb1^{Cre/+}$ (n = 7). Results were combined from four independent experiments.

(C) Flow cytometry representative plot of GC B cells in $Cd23^{Cre/+}$ and $Dot1l^{fl/fl}Cd23^{Cre/+}$ mice d7 post-immunization with NP-KLH in alum.

(D and E) Assessment at d7 and d28 post-immunization for frequency (D) and number (E) of splenic CD19$^+$IgD$^-$NP$^+$CD95$^+$ GC B cells.

(F and G) Representative histological analyses d7 post-immunization: B220 (red) and PNA (blue) (F) and B220 (red) and IgG1 (blue) (G). Scale bars, 100 μm.

(H) Flow cytometry representative plot of NP$^+$IgG1$^+$CD38$^+$ memory B cells.

(I and J) Frequency (I) and total number (J) of splenic memory B cells.

(K and L) Enzyme-linked immunosorbent spot (ELISpot) analysis of IgG1$^+$NP$^+$ BM ASCs (K) and serum NP$^+$IgG1 antibody (L), d28 post-immunization.

n = 6 (d7) and n = 7 (d28) per genotype; combined from two independent experiments per time point. Data are represented as mean ± SEM. *p < 0.05; **p < 0.01; ***p < 0.001.

See also Figures S1, S2, and S3.

was essential for the establishment of humoral memory following T-dependent immunization.

DOT1L Is Required for GC B Cells in Response to the Th1-Cell-Biased Influenza Infection

Inhibition of DOT1L in T helper (Th) cells results in an increase in both Th1 cells and interferon gamma (IFNγ) production *in vitro* (Scheer et al., 2019). B cells also have tailored functional responses to either Th1-cell-biased or Th2-cell-biased stimuli, and although transcription factor expression is associated with dichotomous responses (Piovesan et al., 2017), it is not known whether histone modifiers regulate specialized B cell function. Given the modulation of Th cell function by DOT1L, we used an influenza model to assess the role of DOT1L in an IFNγ-mediated B cell response and to determine whether the role of DOT1L in B cells is generalizable across different types of responses. *Cd23*^{cre/+} and *Dot1l*^{f/f}*Cd23*^{cre/+} mice were infected with the H3N2 HKx31 influenza virus. B cell differentiation was assessed in the spleen and draining (mediastinal) lymph node at d8 and d14 post-infection. Concordant with responses to immunization (Figure 1), DOT1L was required for B cells to mount an effective response to influenza. In the absence of DOT1L, there was a ≥5-fold decrease in splenic GC B cells (Figures S2C–2E) and a similar reduction of GC B cells in the lymph node (Figures S2F and 2G). Those GC B cells that remained were examined for isotype switching to IgG2c and were found to be ~2-fold decreased on a per GC B cell basis (Figure S2H). Finally, we excluded aberrant skewing of immunoglobulin isotypes by assessing Th2-associated IgG1 production in influenza-infected (Th1-cell-biased) mice and, conversely, Th1-associated IgG2c production in NP-KLH-immunized (Th2-cell-biased) mice. In both cases, antibody production of both isotypes was significantly reduced in the absence of DOT1L, and thus, there was no evidence of aberrant Th-cell-biased responses (Figures S2I and S2J, respectively). Therefore, DOT1L was essential for B cells to mount an effective GC reaction during either Th1- or Th2-cell-biased responses.

DOT1L Is Required for Isotype-Switched Plasmablast Formation *In Vivo*

During the early phase of a T-dependent response, activated B cells either migrate back into follicles to form GC or can form foci of proliferating extrafollicular plasmablasts secreting low-affinity unswitched (IgM) and switched (IgG1) isotypes. As GCs were unable to form in the absence of DOT1L, we asked whether this was specific to GC B cell differentiation or whether plasmablast differentiation was also abrogated *in vivo*. *Cd23*^{cre/+} and *Dot1l*^{f/f}*Cd23*^{cre/+} mice were immunized with NP-KLH in alum, and splenic plasmablasts (B220^{lo}CD138⁺ cells) were assessed at d7 (Figure 2A). In the absence of DOT1L, there was a 3-fold reduction in plasmablasts (Figures 2B and 2C). Although a small population of plasmablasts remained in *Dot1l*^{f/f}*Cd23*^{cre/+} mice, these cells had not switched to IgG1 (Figures 2D and 2E). Furthermore, an assessment of antigen-specific ASCs revealed that NP-specific IgG1⁺ ASCs were absent from *Dot1l*^{f/f}*Cd23*^{cre/+} mice (Figures 2F and 2G) and that the NP-binding IgG1 antibody was not detected in serum (Figure 2H). In contrast, there was little difference in NP-specific IgM ASCs (Figure 2I) and

only a small reduction in NP-binding serum IgM (Figure 2J). Although this was consistent with a defect in isotype switching, it may instead reflect the timing of DOT1L function. That is, the defect observed in DOT1L-deficient mice may have occurred after the formation of IgM⁺ plasmablasts in this model. Lastly, we also assessed the formation of plasmablasts during an influenza infection. Plasmablasts in both spleen (Figures 2K and 2L) and mediastinal lymph node (Figures 2M and 2N), as well as serum IgG2c (Figure 2O), were significantly reduced. Together, these data demonstrated an absolute requirement for DOT1L for GC B cell and isotype-switched plasmablast formation in both Th2- and Th1-cell-biased responses.

DOT1L Is Required for Mounting a B Cell Response Independent of T Cells or GCs

The results generated thus far revealed that DOT1L activity was important for establishing a GC and plasmablast response post-immunization with a T-dependent antigen. However, it remained unclear if DOT1L was required for B cell responses that formed independently of T cell help or GCs or possibly promoted the T-independent plasmablast pathway. To investigate these questions in more detail, *Cd23*^{cre/+} and *Dot1l*^{f/f}*Cd23*^{cre/+} mice were immunized with NP-Ficoll in PBS, a type 2 T-independent antigen. Both antigen-specific IgM⁺ (Figure 2P) and IgG3⁺ ASCs (Figures 2Q), as well as the circulating NP-binding IgM (Figure 2R) and IgG3 (Figure 2S) antibody, were significantly reduced in the absence of DOT1L. Interestingly, there was a stronger defect in IgM in the T-independent response (Figure 2R) than the T-dependent response (Figure 2J). This may be due to the significant reduction in marginal zone B cells in *Dot1l*^{f/f}*Cd23*^{cre/+} unimmunized mice compared to that in *Cd23*^{cre/+} mice (Figure S2A), which would likely contribute to the defect in IgM antibody formed in response to NP-Ficoll. In contrast, the frequency of follicular B cells was minimally affected by DOT1L deficiency (Figure S2A). Nevertheless, these data demonstrate that DOT1L is required for effective B cell differentiation into ASCs and antibody production in both T-dependent and T-independent responses.

DOT1L Deficiency Alters the Expression of Genes Required for Effective B Cell Responses *In Vivo*

The next series of experiments were undertaken to delineate how DOT1L regulates B cell fate. Histone modifiers have been linked with cell cycle regulation (Béguelin et al., 2017; Caganova et al., 2013). We used two approaches to determine whether DOT1L-deficient B cells were unable to be activated, had a proliferative defect, and/or were prone to undergo apoptosis. In the first approach, we compared cell trace violet (CTV)-labeled B cells isolated from *Cd23*^{cre/+} and *Dot1l*^{f/f}*Cd23*^{cre/+} mice stimulated *in vitro* with CD40L, IL-4, and IL-5 (Figures S2K–S2Q). In the second approach, we incubated stimulated CTV-labeled wild-type B cells with a small molecule inhibitor to DOT1L (Scheer et al., 2019; Figures S2R–S2U). In both cases, proliferation was not significantly blocked in the absence of DOT1L (Figures S2K–S2M, S2R, and S2S). Interestingly, there was a significant increase in DOT1L-deficient B cells that differentiated into plasmablasts (Figures S2N and S2O), although there was no difference in Blimp-1 expression within CD138⁺ (Figure S2P) or
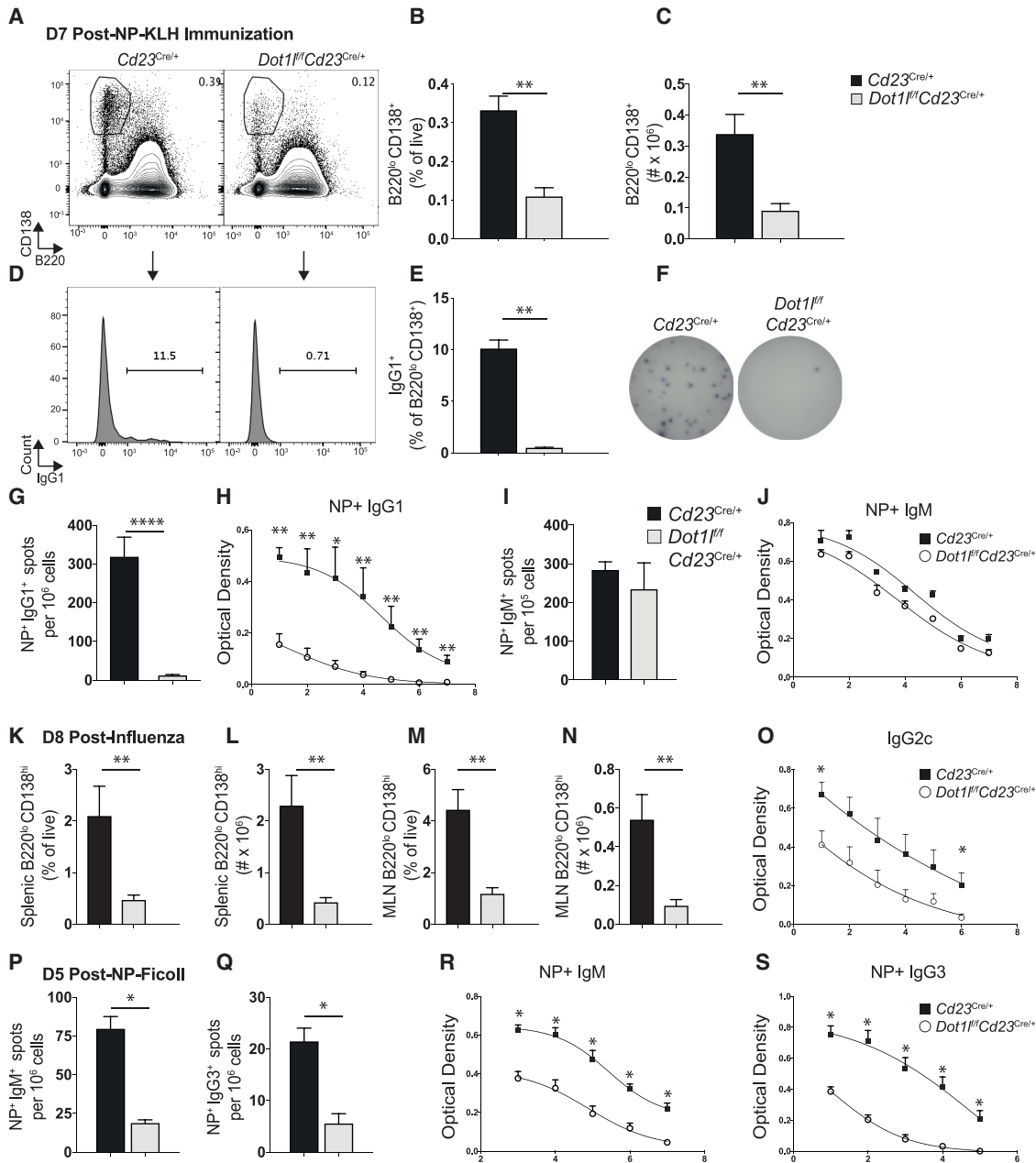
Figure 2. DOT1L Plays a Key Role in the Formation of Class-Switched Splenic ASCs

(A) Flow cytometry representative plot of B220^{lo}CD138$^+$ cells in the presence or absence of Dot1L d7 post-immunization with NP-KLH in alum.

(B and C) Frequency (B) and number (C) of B220^{lo}CD138$^+$ cells in *Cd23*$^{Cre/+}$ and *Dot1l*$^{f/f}$*Cd23*$^{Cre/+}$ mice.

(D and E) Flow representative plot (D) and frequency (E) of IgG1$^+$ cells within the B220^{lo}CD138$^+$ population.

(F–J) ELISpot analysis of splenic NP$^+$IgG1$^+$ ASCs (F and G), serum NP$^+$IgG1 antibody (H), ELISpot analysis of splenic NP$^+$IgM$^+$ ASCs (I), and serum NP$^+$IgM antibody at d7 post-immunization (J). n = 6 (d7) and n = 7 (d28) per genotype.

(K–N) *Cd23*$^{Cre/+}$ and *Dot1l*$^{f/f}$*Cd23*$^{Cre/+}$ mice were infected with HKx31 influenza virus and assessed d8 and d14 post-infection for frequency (K) and number (L) of splenic B220^{lo}CD138$^+$ cells and for frequency (M) and number (N) of mediastinal lymph node B220^{lo}CD138$^+$ cells.

(O) Serum IgG2c at d14 post-infection. n = 6–7 per genotype.

(P–S) *Cd23*$^{Cre/+}$ and *Dot1l*$^{f/f}$*Cd23*$^{Cre/+}$ mice were immunized with NP-Ficoll and assessed d5 post-immunization. ELISpot analysis of splenic NP$^+$IgM$^+$ ASCs (P) and NP$^+$IgG3$^+$ ASCs (Q). Serum NP$^+$ IgM (R) and serum NP$^+$ IgG3 antibody (S).

n = 6 per genotype. Experiments combined from two independent experiments per time point. Data are represented as mean ± SEM. *p < 0.05; **p < 0.01; ****p < 0.0001.

Related to Figures S2 and S3.

CD138⁻ (Figure S2Q) populations. There was a small but non-significant increase in the percentage (Figure S2T) but not number (Figure S2U) of B cells differentiating into plasmablasts in the presence of a small molecule inhibitor. Together with the ability of DOT1L-deficient B cells to produce an early wave of plasmablasts in a T-dependent response *in vivo* (Figure 2J), these approaches demonstrated that DOT1L-deficient B cells were able to divide and differentiate *in vitro*. Thus, humoral responses were not prematurely aborted due to an intrinsic lack of cell proliferation in DOT1L-deficient B cells.

We next confirmed the target histone modification regulated by DOT1L in B cells. Specifically, we determined whether conditional deletion of DOT1L would result in a reduction of global H3K79me2 in B cell subsets. Splenic IgD⁺ and IgD⁻ B cells were sort-purified from immunized *Cd23*^cre/+ and *Dot1*^f/fCd23^cre/+ mice. As expected, in the absence of DOT1L, there was a global decrease in H3K79me2 in B cell subsets (Figures S3A and S3B). Thus, these results confirmed that DOT1L mediates H3K79 methylation in B cells.

This finding led us to investigate whether transcriptional programs were altered in activated B cells. Our strategy was to enrich for the immediate gene regulatory events, without the compounded impact of the absence of GC and memory B cell populations observed at d7 (Figure 1). Thus, we investigated gene expression changes in CD19⁺IgD⁺ naive B cells and CD19⁺IgD⁻ B cell subsets d4 post-immunization, with the latter population being enriched in activated B cells during an immune response. At this time point, there was little difference in the frequency (Figure S3C) or number (Figure S3D) of antigen-specific B cells in DOT1L-deficient compared to DOT1L-sufficient mice; in fact, there was a small but significant increase in DOT1L-deficient CD19⁺IgD⁻ B cells (Figure S3E). In contrast to plasmablasts generated *in vitro* (Figure S2), we did not observe a significant difference in plasmablasts at this time point (Figure S3F). Given the clear absence of antigen-specific B cells by d7, we assessed whether B cells at this earlier time point were more likely to be undergoing apoptosis. This was not the case. The frequency of caspase⁺ cells within the CD19⁺IgD⁻ subset was reduced in *Dot1*^f/fCd23^cre/+ mice compared to controls (Figure S3G) and was unchanged in the antigen-specific population (Figure S3H) and in plasmablasts (Figure S3I).

Gene expression was assessed by RNA sequencing of B cell subsets sort-purified d4 post-immunization with NP-KLH in alum. As expected, the greatest differences were observed between CD19⁺IgD⁺ (naive) and CD19⁺IgD⁻ (activated) B cells and then between control and DOT1L-deficient cells (Figure S4A). Of note, the majority of genes differentially expressed were upregulated in DOT1L-deficient CD19⁺IgD⁺ naive B cells compared to control naive B cells, with only 5 genes downregulated (Figures 3A and 3B). In contrast, 30 genes were downregulated in DOT1L-deficient CD19⁺IgD⁻ B cells compared to controls (Figures 3C and 3D), correlating to the association of H3K79me2 with actively transcribed genes during cell differentiation (Steger et al., 2008). There were 37 genes that overlapped between datasets (Figure S4B). Of these common genes, the vast majority (89%) were upregulated in the absence of DOT1L, with downregulated genes almost solely restricted to CD19⁺IgD⁻ B cells (Figures S4C, S4D, and S4E, respectively).

Multiple genes associated with B cell signaling and migration, such as *Ackr2*, *Ackr4*, *GCsam*, *S1pr2*, and *Tnfrsf17*, were upregulated in B cells from *Cd23*^cre/+ upon activation, compared to naive B cells, but were not expressed in either DOT1L-deficient subsets (Figures 3C and 3E). Chemokine receptors expressed on B cells regulate their ability to migrate in response to chemokine gradients present in the microenvironment (Lu and Cyster, 2019). S1PR2 (the G-protein-coupled sphingosine-1-phosphate receptor encoded by *S1pr2*) is critical for B cell confinement in the GC (Green and Cyster, 2012). Correspondingly, DOT1L-deficient B cells were significantly impaired in their ability to migrate to S1P, compared to DOT1L-sufficient B cells (Figure S4F). The atypical chemokine receptors Ackr2 and Ackr4 have been linked to the regulation of B cell migration (Hansell et al., 2011; Kara et al., 2018), with enforced expression of Ackr4 reducing B cell migration toward CCL21, a CCR7 ligand (Kara et al., 2018). DOT1L-deficient B cells, which had a reduction in *Ackr4*, had a small but non-significant increase in migration to CCL21 (Figure S4F). Although we did not observe an increase in GCs observed in Ackr4-deficient (Kara et al., 2018) and S1PR2-deficient (Green and Cyster, 2012) mice, we hypothesized that disruption of multiple genes associated with localization may be correlated with defective humoral responses in *Dot1*^f/fCd23^cre/+ mice *in vivo*.

In other cell types, DOT1L function has been linked with inhibiting inappropriate differentiation (Wong et al., 2015). Thus, we interrogated whether the expression of transcription factors that regulate differentiation steps in B cells, such as *Bcl6* and *Irf4* (Dent et al., 1997; Klein et al., 2006; Willis et al., 2014), was dysregulated. Although there was no observable difference in gene expression of these transcription factors as assessed by RNA sequencing (data not shown), DOT1L-deficient B cells had a reduced capacity to upregulate BCL6 protein compared to DOT1L-sufficient B cells (Figures 3F and 3G). At d4 post-immunization, B cells from *Dot1*^f/fCd23^cre/+ mice that displayed GC markers (CD95^hiCD38^loIgD^lo) upregulated BCL6 (4.1-fold over naive cells; Figure 3G) but not to the same extent as the equivalent subset from *Cd23*^cre/+ mice (7.6-fold over naive cells; Figure 3G). However, this reduction was not due to lower BCL6 expression in all GC-phenotype cells. The frequency of BCL6⁺ cells within the CD95^hiCD38^loIgD^lo population was significantly reduced in DOT1L-deficient B cells compared to DOT1L-sufficient B cells (Figure 3H). Furthermore, within the BCL6⁺ GC-phenotype subset, BCL6 expression was equivalent between *Dot1*^f/fCd23^cre/+ and *Cd23*^cre/+ mice (Figure 3I). Together, these data reveal the modulation of transcriptional programs that occurs in the absence of DOT1L.

DOT1L Regulates Localization of Activated B Cells during a Humoral Response

During the first ~4 days of an immune response, B cells migrate to the T:B cell border and the interfollicular zone before moving back into the follicle to establish GCs (Chan et al., 2009; Kerfoot et al., 2011; Kitano et al., 2011). To gain further insight into the networks of genes regulated by DOT1L during early B cell responses, ingenuity pathway analysis (IPA) was performed. Notably, IPA identified cellular movement, cell signaling, and DNA replication and repair as the top three functions
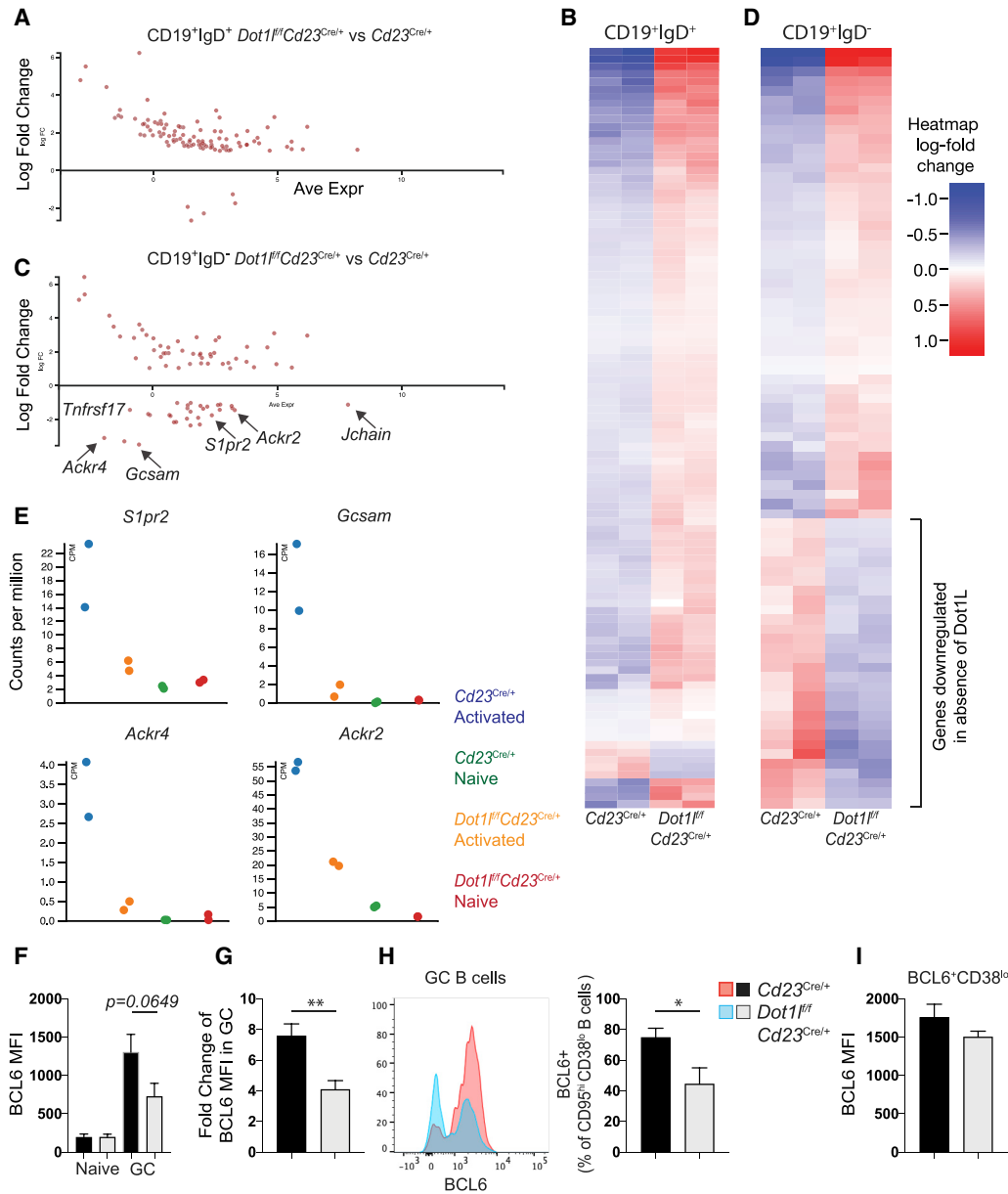
Figure 3. DOT1L Deficiency Modulates the Expression of Genes Underpinning B Cell Responses

(A–D) RNA sequencing data: each sample is an independent sample obtained from CD19+IgD+ or CD19+IgD− B cells sort purified from either *Dot1l*^f/f^*Cd23*^Cre/+^ or *Cd23*^Cre/+^ mice d4 post-immunization with NP-KLH in alum.

(A) MA plot for CD19+IgD+ samples. Shown is the average expression versus log fold change of *Dot1l*^f/f^*Cd23*^Cre/+^ compared to *Cd23*^Cre/+^ samples. A false discovery rate (FDR) cutoff of 0.01 and absolute log fold change of 1 were applied.

(B) Heatmap of CD19+IgD+ B cell data (Table S1); each column is an independent sample.

(C) MA plot for CD19+IgD− samples.

(D) Heatmap of CD19+IgD− B cell data (Table S2).

(E) Plots showing count per million for individual genes for "naive" (CD19+IgD+) and "activated" (CD19+IgD−) samples.

(F) BCL6 geometric mean fluorescence intensity (MFI) in naive and GC B cells.

(G) Fold change of geometric MFI in GC over naive B cells.

(H) Representative plot and frequency of GC B cells that are BCL6+.

(I) BCL6 geometric MFI in BCL6+CD38+CD19+IgD^lo^ B cells.

n = 5–6 per genotype, combined from two independent experiments. Data are represented as mean ± SEM. *p < 0.05; **p < 0.01.

Related to Figure S4 and Tables S1 and S2.

A

Molecular and Cellular Function	# Molecules
Cellular Movement	26
Cell-to-cell Signalling and Interaction	22
DNA Replication, Recombination and Repair	6
Cellular Assembly and Organisation	12
Cell Morphology	15

B

C

B220 CD4/CD8 BCL-6

D
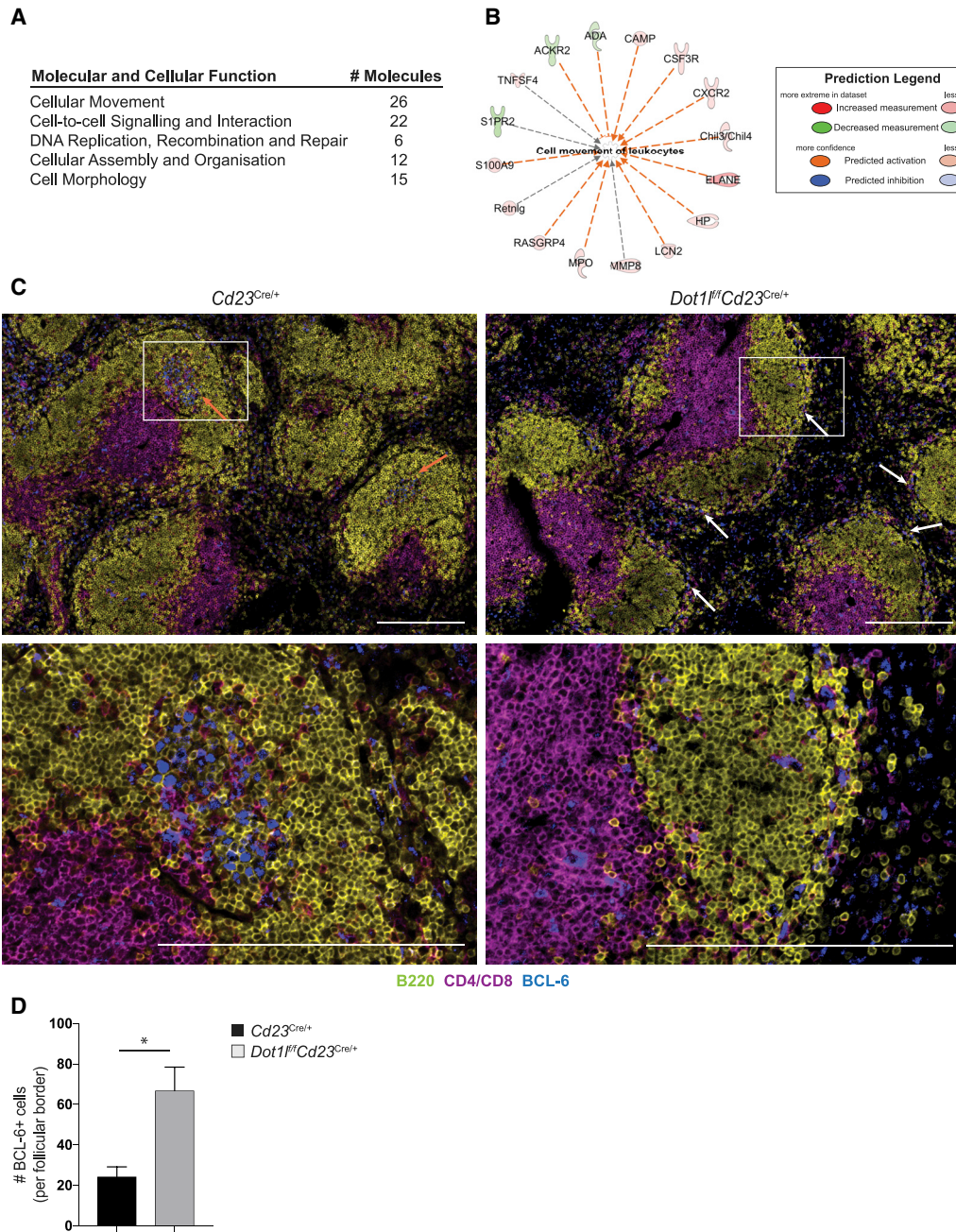
Figure 4. DOT1L Regulates Localization of Activated B Cells during a Humoral Response
(A) IPA analysis of differentially expressed genes in CD19$^+$IgD$^-$ samples. Summary of top molecular and cellular function regulated by Dot1l.
(B) Prediction analysis of differentially expressed genes involved in leukocyte movement.
(C) Representative histological analyses d4 post-immunization: B220 (yellow), CD4/CD8 (magenta), and BCL6 (blue). Scale bars, 100 μm.
(D) Quantitation of BCL6$^+$ cells in the outer edge of follicles.
Data are represented as mean ± SEM. *p < 0.05.
Related to Figure S4.

dysregulated in the absence of DOT1L (Figure 4A). Further analysis revealed networks of molecules involved in cell migration (Figure 4B) and B cell responses (Figure S4G). To investigate the effect of changes in these molecules, we assessed the local-

ization of cells *in vivo* d4 post-immunization. In accordance with transcriptomic data, DOT1L deficiency resulted in altered positioning of B cells within the spleen at the critical time juncture of nascent GC formation *in vivo*. In *Cd23*$^{cre/+}$ mice, BCL6$^+$

B and T cells were observed in the follicle in nascent GC (Figure 4C, orange arrows), consistent with previous studies (Kerfoot et al., 2011; Kitano et al., 2011). In DOT1L-deficient mice, BCL6^{+} cells were detectable, confirming that upregulation of BCL6 in the early stages of the response could occur in *Dot1l^{f/f}Cd23*^{cre/+} mice (Figure 4C). Yet, in contrast to *Cd23*^{cre/+} mice, DOT1L-deficient BCL6^{+} cells did not cluster in the follicle. Instead, BCL6^{+} cells in *Dot1l^{f/f}Cd23*^{cre/+} mice were observed to be located mainly outside the B220[+] follicles (Figure 4C, white arrows). Specifically, BCL6^{+} cells were located in the outer edge of the follicle, potentially in the marginal zone, as well as in extrafollicular areas (Figures 4C), with quantitation revealing a >3-fold increase in BCL6^{+} cells positioned in the outer edge of the follicle in *Dot1l^{f/f}Cd23*^{cre/+} compared to *Cd23*^{cre/+} mice (Figure 4D). Additionally, more B220^{+} cells were observed to penetrate into the T cell zone in the absence of DOT1L (Figure 4C).

It was possible that background responses to environmental antigens were the cause of the histological differences observed. Therefore, we subcutaneously immunized *Cd23*^{cre/+} and *Dot1l^{f/f}Cd23*^{cre/+} mice with NP-KLH in alum and assessed draining and non-draining lymph nodes to confirm the location of B cells responding to the immunogen. At d5 post-immunization, no BCL6^{+} cells were detectable in the non-draining lymph node (data not shown). In contrast, nascent GCs were detected in *Cd23*^{cre/+} mice in the draining lymph node, whereas no clusters of BCL6^{+} cells in *Dot1l^{f/f}Cd23*^{cre/+} mice were detected in the follicle, but instead they were detected at the outer edge of the follicle (Figure S4H), concordant with the splenic results. Thus, dysregulation of a network of genes involved in cellular migration in *Dot1l^{f/f}Cd23*^{cre/+} mice correlated with altered localization in the spleen and lymph node during the initial stage of an immune response. Taken together, this study establishes DOT1L as a pivotal regulator of B cell development, antigen-driven B cell localization, B cell differentiation, and formation of long-lived humoral immune memory.

Elucidation of the critical histone modifiers that regulate B cell fate and function has significant implications for translational studies. In particular, dissecting the role of DOT1L in cellular biology is vital for understanding the biological effects of clinical intervention with DOT1L inhibitors. A DOT1L small molecule inhibitor is currently in clinical trials for the treatment of *MLLr*s (Stein and Tallman, 2015). Our results suggest that sustained inhibition of DOT1L could have an impact on B cell progenitors and the ability of the humoral system to respond to infection. Furthermore, the critical role of DOT1L in multiple stages of B cell biology may indicate that DOT1L could be an important target for other B-cell-derived cancers. For example, DOT1L was identified in a screen of patients with diffuse large B cell lymphoma (Szablewski et al., 2018). This finding raises the possibility that targeting DOT1L in GC-B-cell-derived lymphomas may be a potential, but as yet unexplored, therapeutic option.

In summary, we have identified DOT1L as a critical and central regulator of B cell biology. Here, we demonstrate that appropriate B cell development, as well as localization and ultimately differentiation during immune responses, requires DOT1L function. This work opens up avenues of investigation to understand the fundamental molecular underpinnings of B

cell responses and determine whether small molecule inhibitors targeting DOT1L may be effective in abrogating B-cell-driven diseases.

STAR★METHODS

Detailed methods are provided in the online version of this paper and include the following:

- KEY RESOURCES TABLE
- RESOURCE AVAILABILITY
  - ○ Lead contact
  - ○ Materials availability
  - ○ Data and code availability
- EXPERIMENTAL MODEL AND SUBJECT DETAILS
  - ○ Mice, immunizations and purification of cells
- METHOD DETAILS
  - ○ Flow cytometry
  - ○ ELISPOT
  - ○ ELISA
  - ○ Immunohistochemistry
  - ○ Immunofluorescence
  - ○ Cell Culture
  - ○ Chemotaxis assay
  - ○ RNA-sequencing and bioinformatics analysis
  - ○ Histone extractions and western blotting
- QUANTIFICATION AND STATISTICAL ANALYSIS

AUTHOR CONTRIBUTIONS

K.L.G.-J. designed research; L.K., A.D.P., L.H., and L.D. performed research; J.R.G. performed research and provided intellectual input; S.S. and C.Z. provided reagents, mice, and intellectual input; and K.L.G.-J. wrote the manuscript.

REFERENCES

Alberghini, F., Petrocelli, V., Rahmat, M., and Casola, S. (2015). An epigenetic view of B-cell disorders. Immunol. Cell Biol. *93*, 253–260.

Arrowsmith, C.H., Bountra, C., Fish, P.V., Lee, K., and Schapira, M. (2012). Epigenetic protein families: a new frontier for drug discovery. Nat. Rev. Drug Discov. *11*, 384–400.

Béguelin, W., Popovic, R., Teater, M., Jiang, Y., Bunting, K.L., Rosen, M., Shen, H., Yang, S.N., Wang, L., Ezponda, T., et al. (2013). EZH2 is required for germinal center formation and somatic EZH2 mutations promote lymphoid transformation. Cancer Cell *23*, 677–692.

Béguelin, W., Rivas, M.A., Calvo Fernández, M.T., Teater, M., Purwada, A., Redmond, D., Shen, H., Challman, M.F., Elemento, O., Singh, A., and Melnick, A.M. (2017). EZH2 enables germinal centre formation through epigenetic silencing of CDKN1A and an Rb-E2F1 feedback loop. Nat. Commun. *8*, 877.

Belz, G.T., Xie, W., Altman, J.D., and Doherty, P.C. (2000). A previously unrecognized H-2D(b)-restricted peptide prominent in the primary influenza A virus-specific CD8(+) T-cell response is much less apparent following secondary challenge. J. Virol. *74*, 3486–3493.

Bernt, K.M., Zhu, N., Sinha, A.U., Vempati, S., Faber, J., Krivtsov, A.V., Feng, Z., Punt, N., Daigle, A., Bullinger, L., et al. (2011). MLL-rearranged leukemia is dependent on aberrant H3K79 methylation by DOT1L. Cancer Cell *20*, 66–78.

Caganova, M., Carrisi, C., Varano, G., Mainoldi, F., Zanardi, F., Germain, P.L., George, L., Alberghini, F., Ferrarini, L., Talukder, A.K., et al. (2013). Germinal center dysregulation by histone methyltransferase EZH2 promotes lymphomagenesis. J. Clin. Invest. *123*, 5009–5022.

Chan, T.D., Gatto, D., Wood, K., Camidge, T., Basten, A., and Brink, R. (2009). Antigen affinity controls rapid T-dependent antibody production by driving the expansion rather than the differentiation or extrafollicular migration of early plasmablasts. J. Immunol. *183*, 3139–3149.

Cooper, L., Hailes, L., Sheikh, A., Zaph, C., Belz, G.T., Groom, J.R., and Good-Jacobson, K.L. (2018). Assessing the role of the T-box transcription factor Eomes in B cell differentiation during either Th1 or Th2 cell-biased responses. PLoS One *13*, e0208343.

Dent, A.L., Shaffer, A.L., Yu, X., Allman, D., and Staudt, L.M. (1997). Control of inflammation, cytokine expression, and germinal center formation by BCL-6. Science *276*, 589–592.

Dobin, A., Davis, C.A., Schlesinger, F., Drenkow, J., Zaleski, C., Jha, S., Batut, P., Chaisson, M., and Gingeras, T.R. (2013). STAR: ultrafast universal RNA-seq aligner. Bioinformatics *29*, 15–21.

Dogan, I., Bertocci, B., Vilmont, V., Delbos, F., Mégret, J., Storck, S., Reynaud, C.A., and Weill, J.C. (2009). Multiple layers of B cell memory with different effector functions. Nat. Immunol. *10*, 1292–1299.

Flynn, K.J., Belz, G.T., Altman, J.D., Ahmed, R., Woodland, D.L., and Doherty, P.C. (1998). Virus-specific CD8+ T cells in primary and secondary influenza pneumonia. Immunity *8*, 683–691.

Geng, H., Brennan, S., Milne, T.A., Chen, W.Y., Li, Y., Hurtz, C., Kweon, S.M., Zickl, L., Shojaee, S., Neuberg, D., et al. (2012). Integrative epigenomic analysis identifies biomarkers and therapeutic targets in adult B-acute lymphoblastic leukemia. Cancer Discov. *2*, 1004–1023.

Good-Jacobson, K.L. (2018). Strength in diversity: Phenotypic, functional, and molecular heterogeneity within the memory B cell repertoire. Immunol. Rev. *284*, 67–78.

Good-Jacobson, K.L. (2019). B cells turn on, tune in with LSD1. Nat. Immunol. *20*, 3–5.

Good-Jacobson, K.L., and Shlomchik, M.J. (2010). Plasticity and heterogeneity in the generation of memory B cells and long-lived plasma cells: the influence of germinal center interactions and dynamics. J. Immunol. *185*, 3117–3125.

Good-Jacobson, K.L., Chen, Y., Voss, A.K., Smyth, G.K., Thomas, T., and Tarlinton, D. (2014). Regulation of germinal center responses and B-cell memory by the chromatin modifier MOZ. Proc. Natl. Acad. Sci. USA *111*, 9585–9590.

Green, J.A., and Cyster, J.G. (2012). S1PR2 links germinal center confinement and growth regulation. Immunol. Rev. *247*, 36–51.

Haines, R.R., Barwick, B.G., Scharer, C.D., Majumder, P., Randall, T.D., and Boss, J.M. (2018). The Histone Demethylase LSD1 Regulates B Cell Proliferation and Plasmablast Differentiation. J. Immunol. *201*, 2799–2811.

Hansell, C.A., Schiering, C., Kinstrie, R., Ford, L., Bordon, Y., McInnes, I.B., Goodyear, C.S., and Nibbs, R.J. (2011). Universal expression and dual function of the atypical chemokine receptor D6 on innate-like B cells in mice. Blood *117*, 5413–5424.

Hatzi, K., Geng, H., Doane, A.S., Meydan, C., LaRiviere, R., Cardenas, M., Duy, C., Shen, H., Vidal, M.N.C., Baslan, T., et al. (2019). Histone demethylase LSD1 is required for germinal center formation and BCL6-driven lymphomagenesis. Nat. Immunol. *20*, 86–96.

Inaba, H., Greaves, M., and Mullighan, C.G. (2013). Acute lymphoblastic leukaemia. Lancet *381*, 1943–1955.

Kara, E.E., Bastow, C.R., McKenzie, D.R., Gregor, C.E., Fenix, K.A., Babb, R., Norton, T.S., Zotos, D., Rodda, L.B., Hermes, J.R., et al. (2018). Atypical chemokine receptor 4 shapes activated B cell fate. J. Exp. Med. *215*, 801–813.

Kerfoot, S.M., Yaari, G., Patel, J.R., Johnson, K.L., Gonzalez, D.G., Kleinstein, S.H., and Haberman, A.M. (2011). Germinal center B cell and T follicular helper cell development initiates in the interfollicular zone. Immunity *34*, 947–960.

Kitano, M., Moriyama, S., Ando, Y., Hikida, M., Mori, Y., Kurosaki, T., and Okada, T. (2011). Bcl6 protein expression shapes pre-germinal center B cell dynamics and follicular helper T cell heterogeneity. Immunity *34*, 961–972.

Klein, U., Casola, S., Cattoretti, G., Shen, Q., Lia, M., Mo, T., Ludwig, T., Rajewsky, K., and Dalla-Favera, R. (2006). Transcription factor IRF4 controls plasma cell differentiation and class-switch recombination. Nat. Immunol. *7*, 773–782.

Krishnamurty, A.T., Thouvenel, C.D., Portugal, S., Keitany, G.J., Kim, K.S., Holder, A., Crompton, P.D., Rawlings, D.J., and Pepper, M. (2016). Somatically Hypermutated Plasmodium-Specific IgM(+) Memory B Cells Are Rapid, Plastic, Early Responders upon Malaria Rechallenge. Immunity *45*, 402–414.

Krivtsov, A.V., Feng, Z., Lemieux, M.E., Faber, J., Vempati, S., Sinha, A.U., Xia, X., Jesneck, J., Bracken, A.P., Silverman, L.B., et al. (2008). H3K79 methylation profiles define murine and human MLL-AF4 leukemias. Cancer Cell *14*, 355–368.

Kwon, K., Hutter, C., Sun, Q., Bilic, I., Cobaleda, C., Malin, S., and Busslinger, M. (2008). Instructive role of the transcription factor E2A in early B lymphopoiesis and germinal center B cell development. Immunity *28*, 751–762.

Law, C.W., Chen, Y., Shi, W., and Smyth, G.K. (2014). voom: Precision weights unlock linear model analysis tools for RNA-seq read counts. Genome Biol. *15*, R29.

Liao, Y., Smyth, G.K., and Shi, W. (2014). featureCounts: an efficient general purpose program for assigning sequence reads to genomic features. Bioinformatics *30*, 923–930.

Lu, E., and Cyster, J.G. (2019). G-protein coupled receptors and ligands that organize humoral immune responses. Immunol. Rev. *289*, 158–172.

Mesin, L., Schiepers, A., Ersching, J., Barbulescu, A., Cavazzoni, C.B., Angelini, A., Okada, T., Kurosaki, T., and Victora, G.D. (2020). Restricted Clonality and Limited Germinal Center Reentry Characterize Memory B Cell Reactivation by Boosting. Cell *180*, 92–106.e111.

Milcarek, C., Albring, M., Langer, C., and Park, K.S. (2011). The eleven-nineteen lysine-rich leukemia gene (ELL2) influences the histone H3 protein modifications accompanying the shift to secretory immunoglobulin heavy chain mRNA production. J. Biol. Chem. *286*, 33795–33803.

Okada, Y., Feng, Q., Lin, Y., Jiang, Q., Li, Y., Coffield, V.M., Su, L., Xu, G., and Zhang, Y. (2005). hDOT1L links histone methylation to leukemogenesis. Cell *121*, 167–178.

Pape, K.A., Taylor, J.J., Maul, R.W., Gearhart, P.J., and Jenkins, M.K. (2011). Different B cell populations mediate early and late memory during an endogenous immune response. Science *331*, 1203–1207.

Pelanda, R., Hobeika, E., Kurokawa, T., Zhang, Y., Kuppig, S., and Reth, M. (2002). Cre recombinase-controlled expression of the mb-1 allele. Genesis *32*, 154–157.

Piovesan, D., Tempany, J., Di Pietro, A., Baas, I., Yiannis, C., O'Donnell, K., Chen, Y., Peperzak, V., Belz, G.T., Mackay, C.R., et al. (2017). c-Myb Regulates the T-Bet-Dependent Differentiation Program in B Cells to Coordinate Antibody Responses. Cell Rep. *19*, 461–470.

Powell, D. (2015). Degust: interactive RNA-seq analysis. https://doi.org/10.5281/zenodo.3258932.

Rankin, L.C., Groom, J.R., Chopin, M., Herold, M.J., Walker, J.A., Mielke, L.A., McKenzie, A.N., Carotta, S., Nutt, S.L., and Belz, G.T. (2013). The transcription factor T-bet is essential for the development of NKp46+ innate lymphocytes via the Notch pathway. Nat. Immunol. *14*, 389–395.

Robinson, M.D., and Oshlack, A. (2010). A scaling normalization method for differential expression analysis of RNA-seq data. Genome Biol. *11*, R25.

Scheer, S., Ackloo, S., Medina, T.S., Schapira, M., Li, F., Ward, J.A., Lewis, A.M., Northrop, J.P., Richardson, P.L., Kaniskan, H.U., et al. (2019). A chemical biology toolbox to study protein methyltransferases and epigenetic signaling. Nat. Commun. *10*, 19.

Steger, D.J., Lefterova, M.I., Ying, L., Stonestrom, A.J., Schupp, M., Zhuo, D., Vakoc, A.L., Kim, J.E., Chen, J., Lazar, M.A., et al. (2008). DOT1L/KMT4 recruitment and H3K79 methylation are ubiquitously coupled with gene transcription in mammalian cells. Mol. Cell. Biol. *28*, 2825–2839.

Stein, E.M., and Tallman, M.S. (2015). Mixed lineage rearranged leukaemia: pathogenesis and targeting DOT1L. Curr. Opin. Hematol. *22*, 92–96.

Strahl, B.D., and Allis, C.D. (2000). The language of covalent histone modifications. Nature *403*, 41–45.

Szablewski, V., Bret, C., Kassambara, A., Devin, J., Cartron, G., Costes-Martineau, V., and Moreaux, J. (2018). An epigenetic regulator-related score (EpiScore) predicts survival in patients with diffuse large B cell lymphoma and identifies patients who may benefit from epigenetic therapy. Oncotarget *9*, 19079–19099.

Tsyganov, K., Perry, A.J., Archer, S.K., and Powell, D. (2018). RNAsik: A Pipeline for Complete and Reproducible RNA-seq Analysis That Runs Anywhere with Speed and Ease. J. Open Source Softw. *3*, 583.

Willis, S.N., Good-Jacobson, K.L., Curtis, J., Light, A., Tellier, J., Shi, W., Smyth, G.K., Tarlinton, D.M., Belz, G.T., Corcoran, L.M., et al. (2014). Transcription factor IRF4 regulates germinal center cell formation through a B cell-intrinsic mechanism. J. Immunol. *192*, 3200–3206.

Wong, M., Polly, P., and Liu, T. (2015). The histone methyltransferase DOT1L: regulatory functions and a cancer therapy target. Am. J. Cancer Res. *5*, 2823–2837.

Zhang, Y., and Good-Jacobson, K.L. (2019). Epigenetic regulation of B cell fate and function during an immune response. Immunol. Rev. *288*, 75–84.

Zhang, J., Dominguez-Sola, D., Hussein, S., Lee, J.E., Holmes, A.B., Bansal, M., Vlasevska, S., Mo, T., Tang, H., Basso, K., et al. (2015). Disruption of KMT2D perturbs germinal center B cell development and promotes lymphomagenesis. Nat. Med. *21*, 1190–1198.

STAR★METHODS

KEY RESOURCES TABLE

REAGENT or RESOURCE	SOURCE	IDENTIFIER
Antibodies		
Anti-CD138 PE (clone 281-2)	BioLegend	Cat # 142504; RRID: AB_10916119
Anti-CD138 BV605 (clone 281-2)	BD Bioscience	Cat # 563147; RRID: AB_2721029
Anti-CD45R (B220) AF488 (clone RA3-6B2)	BioLegend	Cat # 103225; RRID: AB_389308
Anti-CD45R (B220) APC-Cy7 (clone RA3-6B2)	BioLegend	Cat # 103224; RRID: AB_313007
Anti-CD45R (B220) AF555 (clone RA3-6B2)	WEHI Antibody Facility	N/A
Anti-IgG1 APC (clone X56)	BD Bioscience	Cat # 550874; RRID: AB_398470
Anti-CD19 APC-Cy7 (clone 6D5)	BioLegend	Cat #115530; RRID: AB_830707
Anti-CD19 Pacific Blue (clone 6D5)	BioLegend	Cat # 115523; RRID: AB_439718
Anti-CD19 PE (clone 6D5)	BioLegend	Cat # 115508; RRID: AB_313643
Anti-IgD AF488 (clone 11-26c.2a)	BioLegend	Cat # 405718; RRID: AB_10730619
Anti-IgD PerCP-Cy5.5 (clone 11-26c.2a)	BD Bioscience	Cat # 564273; RRID: AB_2738722
Anti-CD95 PE-Cy7 (clone Jo2)	BD Bioscience	Cat # 557653; RRID: AB_396768
Anti-CD38 Pacific Blue (clone 90)	BioLegend	Cat # 102720; RRID: AB_10613468
Anti-IgG2a/2b FITC (clone R2-40)	BD Bioscience	Cat # 553399; RRID: AB_394837
Anti-CD43 APC (clone S11)	BioLegend	Cat # 143207; RRID: AB_11149489
Anti-CD249 (BP1) PE (clone BP-1)	BD Bioscience	Cat # 553735; RRID: AB_395018
Anti-CD24 BV421(clone M1/69)	BioLegend	Cat # 101825; RRID: AB_10901159
Anti-IgM AF488 (clone RMM-1)	BioLegend	Cat # 406522; RRID: AB_2562859
Anti-CD169 (MOMA-1) FITC (clone 3D6.112)	Bio-Rad	Cat # MCA884F; RRID: AB_324246
Anti-CD23 AF488 (clone B3B4)	BioLegend	Cat # 101609; RRID: AB_493362
Anti-CD21/CD35 APC (clone 7G6)	BioLegend	Cat # 123412; RRID: AB_2085160
Anti-CD11b APC-Cy7 (clone M1/70)	TONBO	Cat # 25-0112; RRID: AB_2621625
Anti-CD3e PE-Cy7 (clone 145-2C11)	eBioscience	Cat # 25-0031-82; RRID: AB_469572
Anti-CD4 A488 (clone GK1.5-7)	WEHI Antibody Facility	N/A
Anti-CD8a A488 (clone 53.6.7)	WEHI Antibody Facility	N/A
Anti-Bcl6 A647 (clone K112-91)	BD PharMingen	Cat #561525; RRID: AB_10898007
Anti-Blimp1 A647 (clone 5E7)	Biolegend	Cat#150004; RRID:AB_2565618
CaspGLOW Fluorescein activated caspase staining kit	ThermoFisher	Cat# 88-7003-42
Goat anti-mouse IgG1 unlabeled (polyclonal)	Southern Biotech	Cat # 1070-01; RRID: AB_2794408
Goat anti-mouse IgG2a unlabeled (polyclonal)	Southern Biotech	Cat # 1080-01; RRID: AB_2794475
Goat anti-mouse IgG2b unlabeled (polyclonal)	Southern Biotech	Cat # 1090-01; RRID: AB_2794517
Goat anti-mouse IgG3 unlabeled (polyclonal)	Southern Biotech	Cat # 1100-01; RRID: AB_2794567
Goat anti-mouse IgA unlabeled (polyclonal)	Southern Biotech	Cat # 1040-01; RRID: AB_2314669
Goat anti-mouse IgM unlabeled (polyclonal)	Southern Biotech	Cat # 1020-01; RRID: AB_2794197
Goat anti-mouse IgG1 HRP (polyclonal)	Southern Biotech	Cat # 1070-05; RRID: AB_2650509
Goat anti-mouse IgG2a HRP (polyclonal)	Southern Biotech	Cat # 1080-05; RRID: AB_2734756

(Continued on next page)

Continued

REAGENT or RESOURCE	SOURCE	IDENTIFIER
Goat anti-mouse IgG2c HRP (polyclonal)	Southern Biotech	Cat # 1079-05; RRID: AB_2794466
Goat anti-mouse IgG2b HRP (polyclonal)	Southern Biotech	Cat # 1090-05; RRID: AB_2794521
Goat anti-mouse IgG3 HRP (polyclonal)	Southern Biotech	Cat # 1100-05; RRID: AB_2794573
Goat anti-mouse IgA HRP (polyclonal)	Southern Biotech	Cat # 1040-05; RRID: AB_2714213
Goat anti-mouse IgM HRP (polyclonal)	Southern Biotech	Cat # 1020-05; RRID: AB_2794201
Goat anti-mouse IgG3 AP (polyclonal)	Southern Biotech	Cat # 1100-04; RRID: AB_2794572
Goat anti-mouse IgG1 AP (polyclonal)	Southern Biotech	Cat # 1070-04; RRID: AB_2794411
Goat anti-mouse IgM AP (polyclonal)	Southern Biotech	Cat # 1020-04; RRID: AB_2794200
Rat anti-mouse CD45R (B220) (clone RA3-6B2)	BD PharMingen	Cat # 550286; RRID: AB_393581
AffiniPure Goat Anti-Rat IgG (H+L) (polyclonal)	Jackson Laboratory	Cat # 112035003; RRID: AB_2338128
Streptavidin Alkaline Phosphatase	Southern Biotech	Cat # 7100-04
Anti-H3 (polyclonal)	Abcam	Cat# ab1791; RRID: AB_302613
Anti-H3K79me2 (polyclonal)	Abcam	Cat# ab3594; RRID: AB_303937
AffiniPure Goat Anti-Rabbit IgG (H+L) HRP (polyclonal)	Southern Biotech	Cat # 4050-05; RRID: AB_2795955
AffiniPure Goat Anti-Mouse IgG (H+L) HRP (polyclonal)	Biorad	Cat # 1706516; RRID: AB_11125547
Bacterial and Virus Strains		
Influenza virus strain HKx31 (H3N2)	A gift from Professors Gabrielle Belz and Stephen Turner	N/A
Biological Samples		
Mouse Tissue	N/A	N/A
Chemicals, Peptides, and Recombinant Proteins		
NP-PE (Conjugated in-house)	Biosearch Technologies (NP)	Cat # N-1110-100
	Invitrogen (PE)	Cat # P801
Peanut Agglutinin	Vector Laboratories	Cat # B-1075
CD40L	R&D Systems	Cat 8230-CL-050
IL4	R&D Systems	Cat # 405-ML-010
IL5	R&D Systems	Cat # 405-ML-005
Cell Trace Violet	Invitrogen	Cat # C34557
SGC0946	SGC	N/A
BD Cytofix	BD Biosciences	Cat#554714
Clarity Max Western ECL Substrate	Biorad	Cat # 1705062; RRID:AB_2036911
O.C.T Compound	Tissue-Tek	Cat# 4583
Critical Commercial Assays		
Fixable Viability Stain 700	BD Horizon	Cat # 564997
AEC Peroxidase (HRP) Substrate Kit	Vector Laboratories	Cat # SK 4200
Vector® Blue Alkaline Phosphatase Substrate Kit	Vector Laboratories	Cat # SK 5300
Deposited Data		
RNA-sequencing data	This paper	GEO: GSE138401
Experimental Models: Organisms/Strains		
Mb1-Cre	Pelanda et al., 2002	N/A
Cd23-Cre	Kwon et al., 2008	N/A
Dot1ltm1a(KOMP)Wtsi	UCDavis KOMP Repository	CSD29070

(Continued on next page)

Continued

REAGENT or RESOURCE	SOURCE	IDENTIFIER
Software and Algorithms		
Flowjo (Treestar)	FlowJo, LLC	https://www.flowjo.com/
Ingenuity Pathway Analysis	QIAGEN	N/A
Degust	Powell, 2015	https://degust.erc.monash.edu/
NIS-Elements	Nikon	https://www.nikon.com/products/microscope-solutions/lineup/img_soft/nis-elements/
ImageJ	National Institutes of Health (NIH)	https://imagej.nih.gov/ij/index.html
Prism	Graph Pad	https://www.graphpad.com/scientific-software/prism/
Zen Black	ZEISS	https://www.zeiss.com/microscopy/int/products/microscope-software/zen.html
Other		
Superfrost Plus Adhesion Microscope Slides	Thermo Scientific	Cat# J1800AMNT

RESOURCE AVAILABILITY

Lead contact
Further information and requests for resources and reagents should be directed to and will be fulfilled by the Lead Contact, Kim Good-Jacobson (kim.jacobson@monash.edu).

Materials availability
Mouse lines generated in this study are available under a Materials Transfer Agreement. Antibody stocks maintained in-house are derived from a commercially available source and are available for purchase from the WEHI Antibody Facility.

Data and code availability
The accession number for the RNA-seq data reported in this study is GEO: GSE138401.

EXPERIMENTAL MODEL AND SUBJECT DETAILS

Mice, immunizations and purification of cells
Mb1-Cre (Pelanda et al., 2002) and *Cd23*-Cre (Kwon et al., 2008) were provided by Michael Reth and Meinrad Busslinger, respectively. To create *Dot1l^{f/f}* mice, we derived mice from DOT1L targeted ES cells (Dot1ltm1a(KOMP)Wtsi) from UCDavis KOMP Repository and crossed them with FLP mice (Monash University). Subsequently, *Dot1l^{f/f}* mice were crossed with *Mb1-Cre* or *Cd23-Cre* (all on C57BL/6 background). Animal procedures were approved by Monash University Animal Ethics Committee and all mice were maintained at the Monash Animal Research Platform. Mice at least 6 weeks of age and mice of either sex were used in this study. Mice were humanely euthanized by hypercapnea. *T-dependent immunization model:* (4-Hydroxy-3-nitrophenyl)-acetyl (NP) hapten was conjugated to Keyhole Limpet Hemocyanin (NP$_{13}$KLH), precipitated on 10% Alum and diluted in sterile PBS to a final concentration of 100 µg/100 µl. *T-independent immunization model:* NP$_{55}$Ficoll was diluted in sterile PBS to a final concentration of 40 µg/100 µl. *Influenza infections:* Mice were inoculated with 1x10^{4}p.f.u. of HKx31 (H3N2) influenza virus, generously provided by Gabrielle Belz and Stephen Turner, as previously described (Belz et al., 2000; Flynn et al., 1998). *Anasthesia:* Isofluorane (2.5%) was used to lightly anesthetize mice for intranasal infections. Mice were monitored to ensure stabilization of breathing and were warmed by a lamp to alleviate suffering if necessary.

METHOD DETAILS

Flow cytometry
Single cells were resuspended in PBS 2% FCS and stained for flow cytometric analysis as previously described (Cooper et al., 2018). Briefly, 5 × 10^6 cells were resuspended in 50 µL of FVS fixable viability stain, diluted 1:1000 in PBS 2% FCS and incubated for 15 min at room temperature in the dark. Samples were then washed with PBS 2% FCS, and then resuspended in 50 µL of indicated antibodies (see Key Resources Table) and incubated at 4°C for 20 min. FcγRII/III (24G2; supernatant) and normal rat serum (Sigma-Aldrich) was used to block non-specific binding. The CaspGLOW active caspase staining kit (ThermoFisher) was used to assess cells that expressed activated caspases. Cells were then washed and resuspended in PBS 2% FCS and data acquired on a BD Fortessa or

LSRIIa and subsequently analyzed using FlowJo (Tree Star). *Sort-purification*: cells were stained with antibodies and purified by FACS Influx (BD), with purity > 98%.

ELISPOT

ASCs of the IgG1, IgG3 and IgM isotype were analyzed by ELISPOT. Multiscreen HA plates (Millipore) were coated overnight at 4°C with $NP_{12}BSA$ for the quantification of NP-specific IgG1^{+} and IgG3^{+} ASCs. An NP_9BSA coat was used to analyze total NP[+]IgM[+] ASCs while NP_1BSA was used to measure high-affinity IgG1^{+} ASCs. Plates were blocked with PBS 1%BSA for 1 h, washed with PBS, and loaded with samples prepared in RPMI 5%FCS, 50 μM 2-Mercaptoethanol and 2mM Glutamine before an overnight incubation at 37°C. Plates were washed with PBS-Tween and distilled water and subsequently incubated for 1 h at 37°C with secondary antibody (IgG1, IgG3 or IgM) conjugated to alkaline-phosphatase (Southern Biotech) for one h. Plates were washed, as before, and developed with the BCiP®/NBT reaction (Sigma-Aldrich).

ELISA

Serum samples from mice immunized with NP-KLH or NP-Ficoll were assessed by coating 96-well high binding plates (Sarstedt), overnight at 4°C, with 5 μg/μl NP_9BSA for IgM[+] antibodies or $NP_{12}BSA$ for all other isotypes. Serum samples from naive mice or influenza-infected mice were analyzed by coating plates with the appropriate isotype-specific capture antibody (Southern Biotech; Table S3). Plates were blocked, the following day, with PBS 1%BSA for 1 h, washed with PBS-Tween and distilled water and then loaded with serially diluted serum samples before a 4-hour incubation at 37°C. Plates were washed again with PBS-Tween and distilled water and then incubated for 1 h at 37°C with the appropriate anti-mouse secondary antibody conjugated to horseradish peroxidase (Southern Biotech; Table S3). Plates were washed and developed with OPD-substrate solution (Sigma-Aldrich). Serum was serially diluted in block and the optical density values for each sample are shown as a non-linear regression (sigmoidal curve fit).

Immunohistochemistry

Spleens from mice immunized with NP-KLH were extracted, 7 days post-immunization, and frozen in OCT (Tissue-Tek). 7 μm sections were cut using a microtome (Leica) at −20°C and fixed with acetone. Staining was performed using described antibodies (Table S3). Slides were viewed under 4X and 10X magnification using an Olympus CKX41 microscope and images were captured with a mounted Nikon DP-12 camera. Raw images were taken using the Nikon NIS-Element software platform while the processing program, ImageJ, was used to add 100 μm scale bars to each image.

Immunofluorescence

Spleens or inguinal lymph nodes were either directly embedded in OCT compound (Tissue-Tek), or first fixed in 4% paraformaldehyde and immersed in 30% sucrose before being embedded in OCT compound (Tissue-Tek). Tissues were cut via microtome (Leica) into 12 μm sections and mounted on Superfrost Plus slides. Sections were fixed with cold acetone (Sigma) and stained as previously described (Rankin et al., 2013) and using indicated antibodies (Table S3). Images were acquired using a LSM780 confocal microscope (Carl Zeiss MicroImaging). The acquisition software was Zen Black 2012. Quantitation of BCL6^{+} B cells was performed using ImageJ; BCL6^{+} T cells were excluded from quantitation shown in Figure 4.

Cell Culture

Deletion model in culture: CD19^{+} naive B cells were isolated using a B cell negative enrichment kit (STEMCELL) from *Cd23*[Cre/+] mice and *Dot1l*[f/f]*Cd23*[Cre/+] mice. B cells were labeled in PBS with 2 μM CTV (Life Technologies) for 10 min at 37°C. Cells were then washed and resuspended in RPMI 5%FCS, 50 μM 2-Mercaptoethanol and 2mM Glutamine. 5×10^4 labeled B cells were cultured with 50ng/mL CD40L (R&D Systems) in combination with 50ng/mL IL-4 and 5ng/mL IL-5 (R&D Systems). *DOT1L inhibitor in culture:* B cells were purified from wild-type mice as above. Purified B cells were labeled with CTV and cultured with LPS and IL-4. Specified wells were treated with either DMSO or a DOT1L inhibitor (SGC0946) diluted in media.

Chemotaxis assay

B cells were isolated using negative B cell isolation kit (Stem Cell) and resuspended in 0.5% FBS, RPMI 1640 at 5×10^5 cells per well. 100 μl/well were added to the upper chamber of transwell plates and transmigrated across 3 μm transwell filters (Corning Costar Corp, NY, USA) for 3 h. Chemotaxis agent CCL21 (Peprotech; 1 μg/mL) diluted in 0.5% FBS, RPMI 1640, or S1P (Sigma; 100nM) diluted in 2% Fatty acid-free BSA, RPMI 1640, were added to the bottom chamber. Post migration, cells were collected, stained for surface markers and analyzed and enumerated by flow cytometry.

RNA-sequencing and bioinformatics analysis

Sort-purified cell subsets were centrifuged, lysed in RLP Buffer (QIAGEN) and passed through a gDNA eliminator spin column (QIAGEN) to remove genomic DNA. The flow-through was passed through a silica-membrane designed to capture RNA (QIAGEN), which was then washed and dried following the manufacturer's recommendations (QIAGEN RNeasy Plus Micro Kit), and eluted in 14 μL of RNase-free H2O. The 8 RNA samples were prepped using the Illumina Truseq stranded mRNA sample preparation kit with the input RNA of 100ng and sequence using Illumina Nextseq 500 Single End 75 cycles high output version2 cartridge. Raw fastq

files were analyzed using the RNAsik pipeline (Tsyganov et al., 2018) using STAR aligner (Dobin et al., 2013) with the GRCm38.p4 Ensembl reference. Reads were quantified using featureCounts (Liao et al., 2014) producing the raw genes count matrix and various quality control metrics. Raw counts were then analyzed with Degust (Powell, 2015), a web tool which performs differential expression analysis using limma voom normalization (Law et al., 2014), producing counts per million (CPM) library size normalization and trimmed mean of M values normalization (Robinson and Oshlack, 2010) for RNA composition normalization. Degust (Powell, 2015) also provides quality plots including classical multidimensional scaling and MA plots. Data are shown with only protein coding genes and with immunoglobulin genes removed. IPA (QIAGEN) was used for the biological functions and pathway analysis of differentially expressed genes.

Histone extractions and western blotting

$1x10^6$ cells were isolated per sample using fluorescence-activated cell sorting and lysed, overnight at $4°C$, in 0.2M HCl. Cell debris was pelleted and the recovered supernatant was treated at $95°C$, for 5 min, in SDS-PAGE loading buffer (250mM Tris-HCl pH 6.8, 10% SDS, 50% Glycerol, 0.05% bromophenol blue, 5% 2-mercaptoethanol). Samples were resolved on a 12% SDS-PAGE and analyzed by western blot using anti-H3 (Abcam ab1791) and anti-H3K79me2 (Abcam ab3594) antibodies. Blots were further stained with Horseradish Peroxidase- conjugated goat anti-mouse (Southern Biotech) or anti-rabbit IgG (H + L) antibodies (Biorad), developed with Clarity Western ECL Substrate (Biorad) and scanned on the ChemiDoc™ Touch Imaging System (Biorad).

QUANTIFICATION AND STATISTICAL ANALYSIS

The Mann-Whitney nonparametric, two-tailed test was used for statistical analyses of all data, with the exception of western blot and chemotaxis data, using GraphPad Prism software. Paired t test was used for statistical analyses of western blot and chemotaxis data, using GraphPad Prism software. All data are presented as the mean ± the standard error of the mean. n = the number of individual mice assessed.